Linearly polarized Cu L_3-edge x-ray-absorption near-edge structure of $Bi_2CaSr_2Cu_2O_8$

A. Bianconi* and S. Della Longa
University of L'Aquila, via San Sisto 20, 67100 L'Aquila, Italy

C. Li,* M. Pompa, A. Congiu-Castellano, and D. Udron
Dipartimento di Fisica, Università degli Studi di Roma "La Sapienza," I-00185 Roma, Italy

A. M. Flank and P. Lagarde
Laboratoire pour l'Utilisation du Rayonnement Electromagnétique (LURE), Bâtiment 209 D, Université Paris Sud, 91405 Orsay, France

(Received 13 February 1991; revised manuscript received 23 July 1991)

The linearly polarized Cu L_3-edge x-ray-absorption near-edge structure (XANES) of $Bi_2Sr_2CaCu_2O_{8+\delta}$ has been measured and the spectra are interpreted by the full multiple-scattering approach in real space. The polarized spectra over a range of 20 eV can be predicted in terms of the one-electron dipole ($\Delta l=+1$) transition Cu $2p\rightarrow\epsilon d$, probing the unoccupied d-like ($l=2$) density of states projected on the Cu site with orbital angular momentum $m_l=0$, 1 in the $\mathbf{E}\|z$ spectra, and the $m_l=2$, 1, and 0 in the $\mathbf{E}\perp c$ spectra. The oscillator strength for the dipole allowed transitions ($\Delta l=-1$) Cu $2p\rightarrow\epsilon s$ is shown to be a factor of 100 weaker than the $2p\rightarrow 3d$ transitions. The Coulomb interaction in the final state between the Cu $2p$ core hole and the excited Cu $3d$ electron is found to be 5.5 eV forming a bound state below the continuum threshold, the well-known Cu L_3 white line. On the contrary, the core hole induces a nearly rigid redshift about 1 eV of the high-energy conduction bands.

I. INTRODUCTION

X-ray-absorption near-edge structure (XANES) is a modern tool for the investigation of complex systems.[1-4] In fact, this spectroscopy provides a site-selective probe of the local structure and of the electronic states in complex materials. The recent development of this experimental method is due to the availability of high-intensity synchrotron radiation x-ray sources that make it feasible to measure high-signal-to-noise-ratio and high-resolution-absorption spectra.

The application of the XANES spectroscopy to the high-temperature superconductors[5-10] is of interest mainly for two reasons: *first,* because XANES spectroscopy is site selective, i.e., it gives unique information on the local electronic structure[7-9] at the different atomic sites in these systems formed by many different atomic species with a complex crystalline structure;[10] *second,* because XANES spectroscopy is a unique direct probe of the orbital angular momentum (defined by the quantum number l) and of its z components (defined by the quantum number m_l) of the unoccupied electronic states. In fact the dipole selection rules $\Delta l=\pm 1$ for the transitions from a core level, with a well-defined orbital angular momentum l_i, select only the final states having the angular momentum $l=l_i\pm 1$. The information on the orbital angular momentum of the unoccupied electronic states of metals cannot be obtained by other experimental methods probing the unoccupied bands such as the inverse photoemission.

A large number of the XANES works published so far concern the K-edge spectra that are due to the $1s\rightarrow\epsilon p$ transitions, therefore they probe the $l=1$ final states (the p-like unoccupied partial density of states). The K-edge polarized cross section provides information on the z components of the orbital angular momentum of the unoccupied conduction states, because for the $\mathbf{E}\|z$ polarization only the p-like ($l=1$) states with orbital angular momentum $m_l=0$ are reached, while for the $\mathbf{E}\perp z$ polarization only the p-like ($l=1$) states with orbital angular momentum $m_l=1$ are reached The multiple-scattering interpretation of the K-edge XANES spectra in the real space[3,4] has been successfully applied to large number of systems,[1,2] and recently it has been proved to be successful for the interpretation of the polarized K-edge XANES of high-T_c superconducting crystals.[11-15]

The L_3-edge XANES spectra are more complex than the K-edge spectra first because two photoabsorption channels are dipole allowed: (i) the $2p\rightarrow\epsilon d$ transitions, probing the $l=2$ final states (the d-like unoccupied partial density of states); (ii) the $2p\rightarrow\epsilon s$ transitions, probing the $l=0$ final states (the s-like unoccupied partial density of states). However, the $2p\rightarrow\epsilon s$ channel is usually weaker than the $2p\rightarrow\epsilon d$ channel by a factor of 10 to 100.

Unique information on the z components of the orbital angular momentum $m_l=0,\pm 1,\pm 2$ of the $l=2$ unoccupied partial density of states can be extracted by polarized L_3-edge XANES spectroscopy. In fact, the dipole selection rules select the unoccupied d-like ($l=2$) density of states projected on the Cu site with orbital angular momentum $m_l=0,1$ in the $\mathbf{E}\|z$ spectra, and the $m_l=0$, $\pm 1,\pm 2$ in the $\mathbf{E}\perp z$ spectra. In the case of metallic systems, such as the high-temperature superconductors, this is a unique direct experimental method providing this key

information; in fact, the ESR spectroscopy is silent, and the absolute value of the magnetic hyperfine shift in the NMR spectroscopy depends both on the Cu $3d$ orbital angular momentum and on crystal effects.

The multiple-scattering approach[1-4] has been used to predict the unpolarized L_3 XANES of some systems, see for example, the classical example of Pd,[1,3] but we are not aware of papers reporting the calculations of the polarized L_3-XANES spectra in order to study the orbital angular momentum m_l of the unoccupied states over a large energy range. Recently Tyson *et al.*[16] have studied and interpreted the role of the electron spin state in the polarized Mo L_2 and L_3 edges in MoS_2O_2, giving a different ratio L_3/L_2 of the white line intensities in the two polarizations.

In this paper we report for the first time the interpretation of the polarized L_3-XANES spectra of a nonisotropic system, $Bi_2Sr_2CaCu_2O_{8+\delta}$, by theoretical calculations of the polarized Cu $2p \rightarrow d$ absorption cross section over a large energy range including the continuum and the bound final states.

The study of the orbital angular momentum of the $3d$ holes is of central interest for understanding the unique electronic properties of the high-T_c superconductors. The application of the Cu L_3-XANES spectra to the determination of the electronic structure of high-temperature superconductors has provided some key information.

First, the experimental study of the variation of the Cu unpolarized L_3-XANES with doping[17-20] has given a direct experimental identification of the additional itinerant states $3d^9\underline{L}^*$, induced by doping in the correlation gap of the insulating system, i.e., for the lack of $3d^8$ states and the oxygen $2p$ (ligand hole $\underline{L}$) character of the charge carriers.

Second, the study of the white line in the polarized $\mathbf{E}\|c$ L_3-XANES spectra have provided evidence for the Cu $3d$ unoccupied states with the orbital angular momentum $m_l=0,\pm1$.[21-25] These results show that the $3d^9\underline{L}^*$ itinerant states, giving the metallic phase, are *not simply* the first ionization state of the insulating antiferromagnetic phase (i.e., the Zhang-Rice singlets[26] where the orbital angular momentum is frozen in the $m_l=2$ symmetry). This point is relevant in high-T_c superconductivity because the modulation of the orbital angular momentum by the carriers can lead to a polaronic coupling with the lattice dynamics and to virtual dipole or quadrupole electronic excitations that could provide the glue for the superconducting pairs.[25]

The quantitative interpretation of the polarized L_3-XANES spectra over a large energy range is a key step to extract detailed information from the XANES spectra.

Here we have studied the superconducting cuprate perovskite $Bi_2Sr_2CaCu_2O_{8+\delta}$, discovered by Maeda *et al.*,[27] with critical temperatures in the range of 70–90 K, which is one of the most interesting high-temperature superconducting systems. The structure of the $Bi_2Sr_2CaCu_2O_{8+\delta}$, crystal has been investigated by neutron and x-ray diffraction[27-32] and by extended x-ray-absorption fine-structure (EXAFS) methods.[33-35] The Cu ion is fivefold coordinated by four planar oxygen atoms O(P) in the CuO_2 plane at distance of about 1.9 Å and by one apex oxygen atom O(A) in the SrO plane forming a distorted Cu square pyramid coordination geometry. Calestani *et al.*[31] have solved the 5×1 superstructure, showing the presence of five different Cu sites, and the EXAFS analysis[33] has pointed out the large Debye-Waller factor for the apex oxygen as well as the distortion of the square plane with two sets of Cu-O(P) distances with an average bond length difference of 0.12 Å.[34,35] There are large differences between the average Cu-O(A) distances reported by several authors, ranging from 2.17 to 2.65 Å from diffraction, and EXAFS data.

The oxygen content in the crystals of $Bi_2Sr_2CaCu_2O_{8+\delta}$ depends on the preparation procedure, also the c axis in different crystals has values ranging from 30.6 to 30.95 Å, but the samples always remain superconductors with a critical temperature modulated in the temperature range from 70 to 90 K. Because the $Bi_2Sr_2CaCu_2O_{8+\delta}$ crystals are stable in a vacuum, they have been the subject of extended experimental investigation. The dispersion of the bands near the Fermi level has been measured by angular resolved photoemission[36,37] and infrared spectroscopy.[38] The one-electron band calculations[39-43] show two bands crossing the Fermi level: the band of Cu $3d_{x^2-y^2}$ ($m_l=2$) and O $2p_x$, O $2p_y$ partial density of states and a second band with contributions from the Bi layers.

A correlation gap between the $3d_i^9+3d_j^9 \rightarrow 3d_i^{10}+3d_j^9\underline{L}_j$ opens up in the $3d$ band, due to the large Cu $3d$-$3d$ intra-atomic hole-hole Coulomb repulsion $U_{dd}\sim6$ eV and for the Cu $3d$-O $2p$ interatomic Coulomb repulsion $U_{dp}\sim1$ eV.[44-47] The correlation gap in the ionic limit is given by the $\Delta+U_{pd}$, where Δ is the energy separation between the $3d^9$ and the $3d^{10}\underline{L}$ configuration. In the superconducting phase additional states $3d^9\underline{L}^*$ are formed in the gap at the Fermi level[21-25] as in other families of high-T_c superconductors.[17-21]

We will show here that the localized character of the Cu $3d$ states shows up in the XANES spectra because it gives a large Coulomb attraction $Q_{cd}=5.5$ eV between the core hole and the Cu $3d$ states, which is nearly the same as $U_{dd}\sim6$ eV. On the other hand, the excitonic attraction $Q_{c\varepsilon}$ between the core hole Cu $2p$ and the delocalized states at the energy ε in the continuum induces only a rigid shift of about 1 eV.

II. EXPERIMENTAL

The Cu L_3 x-ray-absorption experiment has been carried out on the Super-ACO storage ring at the Laboratoire pour l'Utilisation du Rayonnement Electromagnetique (LURE), Orsay, France. A double-crystal $10\bar{1}0$ beryl monochromator with an energy resolution of about 0.35 eV at 900 eV has been used. The maximum of the white line of the Cu L_3 absorption spectrum at 931.2 eV in CuO has been used to calibrate the photon energy scale.

The absorption coefficient has been measured by total electron yield method, i.e., by recording the intensity of the electrons emitted by the sample surface accelerated

by a positive voltage toward a channeltron electron multiplier put at 900° from the x-ray beam direction. The thickness of the probed surface layer is given by the average electron escape depth of all emitted electrons with an energy spectrum extending from a maximum at 2–4 eV, due to secondary electrons, to the energy of direct valence-band photoemitted electrons with kinetic energy $h\nu$-ϕ, where ϕ is the metal work function. Because the mean free path is maximum for the low-energy secondary electrons and their number is much larger than the direct photoelectrons and Auger electrons, the average thickness is determined by the electron escape depth of secondary electrons of about 100–200 Å.

The crystals have been cleaved with the surface normal z axis parallel to the c axis of the crystal, i.e., with the surface xy plane parallel to the ab plane of the crystal (or to the CuO_2 planes). The crystals have been mounted in the experimental chamber with the c axis in the horizontal zy plane, and they could be rotated around the vertical x direction. The incident angle of the collimated x-ray-beam direction with the sample normal was measured. The polarized x-ray-absorption spectra (XAS) of the single crystals using synchrotron radiation linearly polarized in the horizontal plane have been recorded with several incidence angles between the electric field **E** of the photon beam and the sample surface normal z (the z axis was taken parallel to the c axis).

The line shape of the white line shows a broadening going from ($\mathbf{E}\perp z$) to ($\mathbf{E}\parallel z$) as measured by studying the changes of the white line of a nonoriented powder sample of CuO with the incidence angle in agreement with Ref. 48, but this effect is so small that it is negligible in comparison with the intrinsic differences between the two polarizations found in the $Bi_2Sr_2CaCu_2O_8$ crystal.

III. RESULTS AND DISCUSSION

A. Polarized Cu L_3-edge XANES spectra

Several oriented $Bi_2Sr_2CaCu_2O_{8+\delta}$ single crystals with a single jump at the critical temperature ($T_c=85$ K) in the resistivity curve have been studied. The investigation of the structure of these oriented crystals by x-ray diffraction shows a single crystallographic 2:2:1:2 phase with the c axis at 30.7 Å.

We report in Fig. 1 the polarized spectra of $Bi_2Sr_2CaCu_2O_{8+\delta}$ obtained by summing many experimentals spectra in order to obtain a good signal-to-noise ratio in the continuum part of the spectrum, between the L_3 and the L_2 white lines at 931.35 and 951.2 eV, respectively.

We have extrapolated the polarized spectra $\mathbf{E}\parallel c$ ($I_\parallel$) and $\mathbf{E}\perp c$. ($I_\perp$), shown in Fig. 1, from the linearly polarized spectra of the crystal measured at several incidence angles of the polarized synchrotron radiation direction beam with the surface normal, 0°, 35°, 55°, and 75°. In order to obtain the extrapolated polarized spectra, we have used the formula

$$I_\phi(\omega)=(\cos\phi)^2 I_\perp(\omega)+(\sin\phi)^2 I_\parallel(\omega)\ ,$$

where $I_\phi(\omega)$ is the normalized experimental spectrum recorded at the incidence angle ϕ as function of the energy ω. The spectra exhibit two isosbestic points at 935.5 and 949 eV. The absorption coefficient has been normalized in such a way that the absorption coefficient of the $\mathbf{E}\parallel c$ polarized spectrum is one at 937 eV. The spectrum in Fig. 1 shows a large dichroism both in the energy region of the white line 928–936 eV as well as in the continuum part in the range 936–949 eV.

The $\mathbf{E}\parallel c$ polarized x-ray-absorption near-edge structure (XANES) spectrum in Fig. 1 exhibits some features $C1$ and $C2$ in the energy range between 935.5 and 949 eV, while the $\mathbf{E}\perp c$ spectrum exhibits a minimum at about 939 eV and a weak structure $D1$ at about 941 eV.

B. Construction of the muffin-tin potential for a finite cluster

In order to understand the XANES spectrum we have calculated the polarized XANES spectra in the frame of the one-electron approximation. The XANES spectra have been calculated in real space using the multiple-scattering formalism.[1–4] In this approach the transition rate of electronic excitations from the Cu $2p$ core to a final state of a cluster of atoms with the absorbing atom at its center is calculated. The final-state wave function of the excited electron is calculated in a potential having the form of nonoverlapping muffin tins.

The first step is the construction of a cluster of neighboring atoms, around the central Cu, starting from atom-

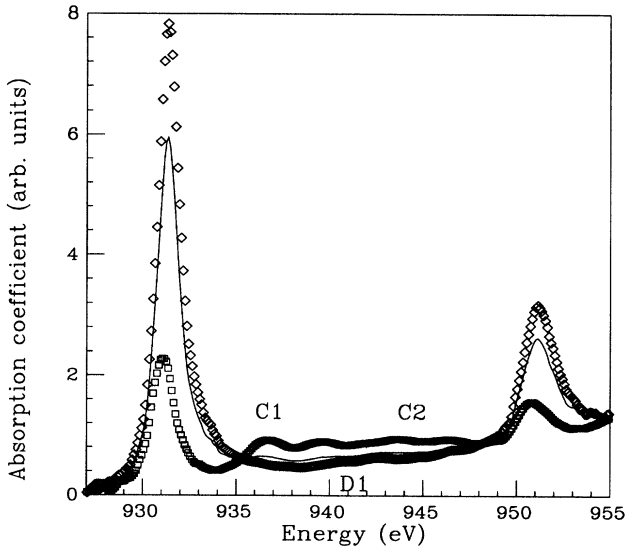

FIG. 1. Polarized $\mathbf{E}\perp c$ (or $\mathbf{E}\parallel ab$) (diamonds) and $\mathbf{E}\parallel c$ (squares) Cu $L_{2,3}$-edge XANES spectra of $Bi_2Sr_2CaCu_2O_{8+\delta}$ measured in the total electron yield mode. The unpolarized spectrum (solid line) measured at the magic incidence angle (35°) is also shown.

ic coordinates given by crystallographic investigations. We have used the atomic coordinates of $Bi_2Sr_2CaCu_2O_{8+\delta}$ from Bordet *et al.*[29] The absorbing Cu atom is the center of the cluster shown in Fig. 2. The cluster is divided into five shells. In Table I we report the distances of the atoms in each shell from Cu and their distance from the CuO_2 plane. The oxygen atoms in the CuO_2 plane are classified as planar oxygen atoms O(P) and the oxygen atoms in the SrO planes are classified as apex oxygen atoms O(A). The cluster includes four Cu ions of the neighbor CuO_4 square planes of the central Cu and one Cu ion from a different CuO_2 plane, as well as one Bi ion belonging to the BiO layers.

We used the Mattheiss prescription to construct the muffin-tin potentials.[3] The calculation of the potential starts from the charge densities for neutral atoms on each site, which were obtained by self-consistent-field atomic calculations of the relativistic Hartree-Fock Slater kind. The charge densities about each atom were superimposed and spherically averaged. By solving Poisson's equation for the Coulomb part of the potential and adding a local exchange-correlation contribution of the $X\alpha$ type with $\alpha=1$, the spherically symmetric potentials in the muffin-tin form were obtained.

The muffin-tin approximation has been thoroughly tested to be rather accurate for XANES applications in a large set of samples.[1,2] The more open the structure, however, the worse the muffin-tin approximation is expected to become because the interstitial region between the muffin-tin spheres, where the muffin-tin approximation makes its worst errors, is larger. The muffin-tin approximation becomes poor, especially when the exact interstitial potential undergoes large variations near its mean value. Therefore, having five different atomic sites, Cu, O, Sr, Ca, and Bi, the present search has been focused to find a set of muffin-tin radii for each atomic species that gives a constant intersphere energy, by keeping the condition for nearly touching and nonoverlapping

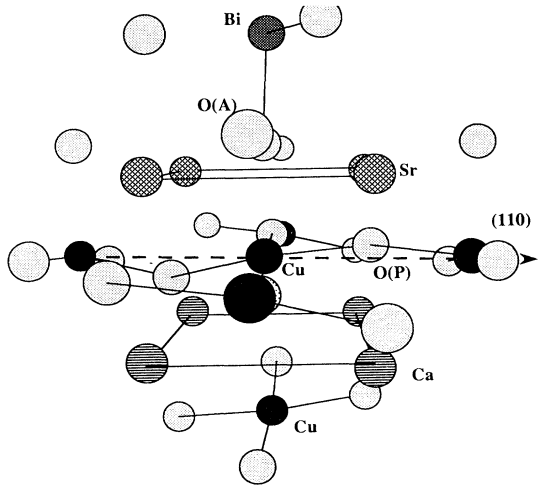

FIG. 2. Structure of the cluster of 38 atoms with the Cu atom in the center used to calculate the XANES spectra. The atoms are grouped in five shells of neighboring atoms. The cluster includes one Cu atom of the neighbor CuO_2 plane and a Bi atom from the BiO plane.

TABLE I. Structure of the five-shell cluster for $Bi_2CaSr_2Cu_2O_8$ (Ref. 29).

Shell	Atom	Number of atoms	Distance from Cu (Å)	Distance from CuO_2 plane (Å)
1	O(P)	1	1.893	−0.42
1	O(P)	1	1.923	−0.42
1	O(P)	1	1.937	+0.21
1	O(P)	1	2.024	+0.21
1	O(A)	1	2.261	+2.261
2	Sr	2	3.19	+1.69
2	Sr	1	3.07	+1.69
2	Sr	1	3.32	+1.69
2	Ca	1	3.12	−1.67
2	Ca	2	3.18	−1.67
2	Ca	1	3.25	−1.67
2	Cu	1	3.35	−3.35
3	O	2	3.5	−2.93
3	Cu	2	3.72	0
3	Cu	2	3.94	0
4	O	2	4.0	−3.56
4	O(P)	4	4.3	+0.21
4	O(P)	4	4.3	−0.42
4	O(A)	2	4.3	+2.26
4	Bi	1	4.37	+4.37
5	O(A)	2	4.56	+2.26
5	O	2	4.7	+4.19

spheres. The intersphere energies near each atomic site i (here called the muffin-tin constants $\overline{V}_{0i}$) of the constructed muffin-tin potentials, were initially determined by taking the average values of the potential in the space between the muffin-tin radius $R_{\mathrm{MT}i}$ and the radius of the Wigner-Seitz spheres. The muffin-tin radius of each atomic species has been chosen looking for a solution giving similar $\overline{V}_{0i}$ in order to minimize the variations of the interstitial potential about its mean value. The average interstitial potential $\overline{V}_0$ for the crystal has been taken as the value of $\overline{V}_{0i}$ for the Cu site. The values of muffin-tin radii $R_{\mathrm{MT}i}$ and the muffin-tin energy constant are given in Table II.

C. The transition rate to final states with selected orbital angular momentum m_l

In Fig. 3 we report the calculated spectra for the different photoionization channels for final states with the $l=2$ and $m_l=0$, $m_l=1$ and $m_l=2$ orbital angular momentum, which can be classified as $(l,m)=(2,0)$, (2,1), and (2,2) final states, where the component of the orbital angular momentum m_l is shortly indicated by m. The zero of the energy scale of the calculated spectra has been taken to be $\overline{V}_0$.

In the XANES multiple-scattering calculation the wave function of all electronic states above the average interstitial potential $\overline{V}_0$ are calculated, and the transition rate for dipole transitions from the Cu $2p$ level is calculated without taking into account whether the valence states are occupied or unoccupied. The Cu $3d$ valence states can be described[49,50] in the single-point-group representations via the standard-model-symmetry-adapted spherical harmonics $Y_{l,m}$. The generalized harmonics transforming according to the four one-dimensional representations of a C_{2v} point group:

$$d_{x^2-y^2},\ (1/\sqrt{2})[Y_{22}(r)+Y_{2-2}(r)]\ ,$$

$$d_{xy},\ (1/\sqrt{2})[Y_{22}(r)-Y_{2-2}(r)]\ ,$$

$$3d_z2,\ Y_{20}(r)\ ,$$

$$d_{xz},\ (1/\sqrt{2})[Y_{21}(r)-Y_{2-1}(r)]\ ,$$

$$d_{yz},\ (1/\sqrt{2})[Y_{21}(r)+Y_{2-1}(r)]\ .$$

Therefore the main peaks in the transition rate from the Cu $2p$ level to the $m_l=2$ valence states shown in Fig. 3 is determined by both the $d_{x^2-y^2}$ and the d_{xy} states. The crystal-field splitting separates the two valence states; therefore the $m_l=2$ spectrum shows a low-energy peak due to the d_{xy} states and a second high-energy peak due to the $d_{x^2-y^2}$ states. The spectrum in Fig. 3 for the $m_l=0$ valence states is determined by the $3d_{z^2}$ valence states. The spectrum in Fig. 3 for the $m_l=1$ valence state probes the $3d_{xz}$ and $3d_{yz}$ valence states.

The Fermi level is found at 11.6 eV above the average interstitial potential $\overline{V}_0$, i.e., at the maximum of the peak for the $m_l=2$ channel in agreement with the fact that only a single Cu $3d$ hole is present in the $Bi_2Sr_2CaCu_2O_8$ sample. All the final states at energy lower than the dashed line in Fig. 3 (the Fermi level) are occupied, and they do not contribute to the experimental absorption spectra. Therefore the white line in the experimental spectrum in Fig. 1 can be assigned to the unoccupied Cu $3d$ states with mainly $m_l=2$ character with some contributions from unoccupied $m_l=0$ states above the Fermi level, while the contribution of the states with $m_l=1$ symmetry is negligible.

In Fig. 4 we report the results of the calculations of the transition rate for the transitions to the final states with selected orbital angular momentum in the continuum above the Fermi level that will give the XANES features in the continuum. The atomic absorption coefficient α_0 calculated for the single muffin-tin potential of the central Cu ion is also shown. The absorption coefficient has been

TABLE II. The muffin-tin radii $R_{\mathrm{MT}i}$(Å) of the elements included in $Bi_2Sr_2CaCu_2O_8$ and the muffin-tin constants $\overline{V}_{0i}$ (eV).

	R_{MT} (Å)		$\overline{V}_{0i}$ (eV)	
Elements	Unrelaxed	Relaxed	Unrelaxed	Relaxed
Cu	0.978	0.952	−20.4664	−21.1979
O	0.915 97	0.941 97	−20.4602	−21.1146
Sr	0.999 3	0.985	−20.4385	−21.1850
Ca	1.331	1.332	−19.2440	−19.2096
Bi	1.05	1.05	−19.7741	−19.8785

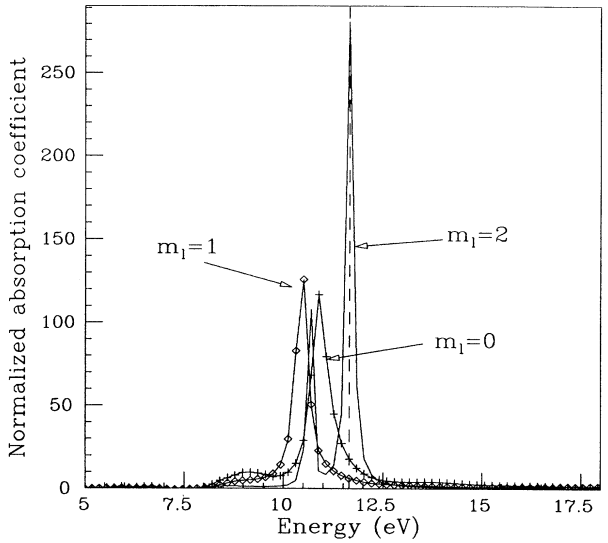

FIG. 3. Calculated photoionization cross section for the transitions from the Cu $2p$ level to the final states with orbital angular momentum $m_l=0$, 1, and 2. The large cross section for the $2p\rightarrow 3d$ transitions gives the strong peaks between 10 and 12.5 eV. In the experimental spectrum only transitions to unoccupied final states above the Fermi level (the dashed vertical line) are expected. The zero of the energy scale of the calculated spectra is chosen at the average interstitial potential $\overline{V}_0$.

TABLE III. Energy of the peaks in the XANES spectra.

	White line ($\mathbf{E}\|c$)	White line ($\mathbf{E}\perp c$)	C_1	C_2	D_1
		Calculated peak positions in the unrelaxed potential			
$(E-\bar{V}_0)$ eV		11.6	13.7	21.2	20.6
$(E-E_0)$ eV		0	2.1	9.6	9
		Calculated peak positions in the relaxed potential			
$(E-\bar{V}_0)$ eV		6.1	12.4	20	17
$(E-E_0)$ eV		−5.5	0.8	8.4	5.3
		Experimental (eV)			
	931.1±0.5	931.3±0.5	936.5±0.5;939.5±0.5	944.±0.5	941±1

normalized to the value of the atomic absorption coefficient $\alpha_{0\infty}$ for the central Cu ion at 50-eV energy above the edge.

We classify the transitions, determining the XANES features, as $2p \rightarrow \varepsilon d$, i.e., to the $l=2$ final states at energies ε in the continuum, to be distinguished from the $2p \rightarrow 3d$ transitions determining the white line.

Following the core-hole excitation, the electrons, in the excited atom, move in a different potential due to the excited electron-hole dipole. The positive nucleus is less screened after removing the core electron; therefore the wave functions of the passive electrons are pulled in toward the nucleus by the attractive interaction, while the core and the passive electrons relax to lower energy. Therefore the description of the final state becomes a many-body problem. In order to reduce the problem to a one-electron problem we have to consider that the excited photoelectron moves in a new potential, which evolves in the time following the rearrangement of the passive electron toward the *fully relaxed* configuration, i.e., the lowest-energy configuration for all other $N-1$ electrons in the presence of the core hole. According to the final-state rule the core-hole relaxation effect can be reduced to a one-electron problem by assuming that the potential attracting the photoelectron is the static potential, where all passive electrons are fully relaxed in the presence of the core hole. Therefore according to the final-state rule the XANES spectra have to be calculated using the fully relaxed potential.

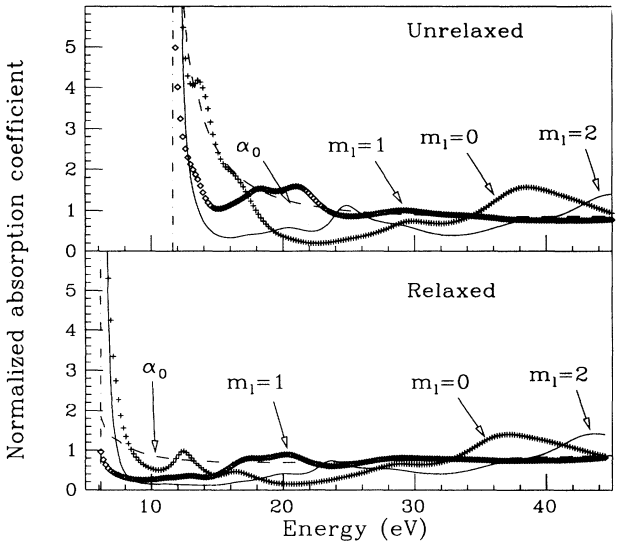

FIG. 4. Calculated photoionization cross section for the $2p \rightarrow \varepsilon d$ transitions to the final states with orbital angular momentum $m_l=0,1,2$ in the continuum, above the Fermi level (upper panel). In the lower part the absorption cross section in the fully relaxed potential in the presence of the core hole is calculated. The atomic absorption $\alpha_0(\omega)$ of the central Cu ion is shown (dashed line). The absorption coefficient has been normalized to the value of the atomic absorption coefficient for the central Cu ion $\alpha_{0\infty}$ at high energy (45 eV). The zero of the energy scale of the calculated spectra is at the average interstitial potential $\bar{V}_0$.

In the $Z+1$ approximation the fully relaxed potential is closely approximated by that of the atom with its Z atomic number increased by one.[1] We have calculated the fully relaxed potential by assuming that the central atom is Zn. The muffin-tin potential of the cluster has been calculated for the relaxed electronic configuration. The results of Cu L_3-edge XANES calculations for the fully relaxed potential are shown in the lower part of Fig. 4.

The effects of the core-hole-induced relaxations on the Cu L_3 XANES moves the Cu $3d$ final states toward lower energy by 5.5 eV, while the εd states in the continuum are moved down by only 1 eV. The Cu $3d$ states are much more localized than the states in the higher conduction band, therefore the overlap with the core hole is much larger than for the higher states. The Coulomb interaction between the Cu $2p$ hole and the Cu $3d$ electron is as large as the Coulomb repulsion between the $3d$ holes in the valence band $U_{dd}=6$ eV. The final result of the core-hole effect on the valence states is that the unoccupied Cu $3d$ states at the Fermi level are split from the higher conduction band, and they form a bound state at −5.5 eV below the predicted continuum threshold. The peaks in the continuum at higher energy than the white line are due to the unoccupied partial density of states with d-like character, and they are shifted only by ~ 1 eV. The first peak beyond the white line, at 14 eV in Fig.

4, is due to the first conduction band above the $3d$ band; it is at 2.1 eV above the continuum threshold E_F in the initial state, and it is moved by the final-state effect at 0.8 eV above E_F.

D. Selection rules in polarized L_3 XANES

The polarized absorption coefficient of a photon $h\nu$ with polarization **E**, for the initial and final states with energies E_i and E_f, respectively, in the dipole approximation is given by

$$\alpha(h\nu)=4\pi^2\alpha h\nu\sum_{if}|\langle\psi_i|\mathbf{E}\cdot\mathbf{r}|\psi_f\rangle|^2\delta(E_f-E_i h\nu) ,$$

where the sum is extended to all many particle final states f such that $E_f-E_i=h\nu$. In the one electron approximation where the initial wave function $\psi_i(r)$ is the Cu $2p$ atomic wave function is given by

$$\psi_{n_i,l_i,m_i,m_s}(r)=R_{n_i,l_i}(r)Y_{l_i,m_i}\chi^{m_s} ,$$

where for the Cu $2p$ electrons $R_{n,l}(r)=R_{2,1}(r)$ satisfies the radial Schrödinger equation, being finite at the origin and zero at the muffin-tin radius R_{MT}, $Y_{1,m_i}(r)(m_i=0,\pm1)$ is the standard spherical harmonic and $\chi^{m_s}(m_s=\pm\frac{1}{2})$ is a two-component spinor describing the two possible spin polarizations of the core electron.[16]

The final-state wave function is the valence-state wave function[49,50] extending over a large cluster of atoms, given in the frame of the group theory by

$$\psi_{n,l,m,m_s}(r)=\sum_{h,l}R_{n,l}(r)\chi_{hl}(r)\chi^{m_s} ,$$

where the radial part of the wave function $R_{n,l}(r)$ extending beyond the site of the absorbing atom and satisfies the same differential equation as the core radial wave function but matches on to the solution outside the atomic-sphere radius R_{MT},[51] $\chi_{hl}(r)$ are symmetry-adapted spherical harmonics that can be expressed in terms of the regular harmonics[52,53] by

$$\chi_{hl}=\sum_m b_{hlm}Y_{l,m}(r)$$

Finally by combining the above expression for the initial and final states and by summing over the spins, the polarized absorption coefficient is given by

$$\alpha(h\nu)=8\pi^2\alpha h\nu\sum_{i,f}|\mathbf{M}_{if}(r)\sum_m b_{hlm}(Y_{l_i,m_i}|\mathbf{E}\cdot\mathbf{r}|Y_{l_f,m_f})|^2\delta(E_f-E_i-h\nu) .$$

Therefore the dipole selection rules for the polarized Cu L_3-XANES spectra are determined by the integral over three spherical harmonics,

$$\sum_{m_i}|\langle Y_{l_i,m_i}(r)|Y_{l_\gamma,m_\gamma}(r)|Y_{l_f,m_f}(r)\rangle|^2 ,$$

where $Y_{l_i,m_i}(r)$ describes the core initial state, $Y_{l_f,m_f}(r)$ the electron final state, and $Y_{l_\gamma,m_\gamma}(r)$ the polarized photon field. The value of each integral is proportional to the $3-j$ Wigner symbols,

$$\begin{pmatrix} l_i & l_\gamma & l_f \\ m_i & m_\gamma & m_f \end{pmatrix}^2 ,$$

which are different from zero under the condition that $m_i+m_\gamma+m_f=0$.[54] For example the dipole selection rule for the Cu $2p\rightarrow3d_{z^2}$ transition for the $\mathbf{E}\|c$ polarization is given by

$$\sum_{m_i}|\langle Y_{1,m_i}(r)|Y_{1,0}(r)|3d_{z^2}\rangle|^2\propto\begin{pmatrix}1&1&2\\0&0&0\end{pmatrix}^2$$

In the $\mathbf{E}\|c$ polarization, $m_\gamma=0$, the dipole matrix element is different from zero only for $m_f=\pm1$, 0 because $m_i=\pm1,0$. The transitions to the $d_{x^2-y^2}$ and d_{xy} valence states, $m_f=\pm2$, are forbidden in the $\mathbf{E}\|c$ polarization, We obtain for the $\mathbf{E}\|c$ spectrum $I_\|(\omega)$ in terms of the partial contributions $I_{l,m}$ to the absorption cross section due to final states with orbital angular momentum l,m,

$$I_\|(\omega)=\tfrac{2}{3}I_{2,0}(\omega)+I_{2,1}(\omega) .$$

In the $\mathbf{E}\perp c$ polarization all final valence states can be reached, but with different probability, for example the relative weight for the $3d_{z^2}$ final state is given by

$$\sum|\langle Y_{1,m_i}(r)|(1/\sqrt{2})[Y_{1,-1}(r)+Y_{1,-1}(r)]|3d_{z^2}|^2 .$$

In conclusion, we obtain for the $\mathbf{E}\perp c$ spectrum $I_\perp(\omega)$ in terms of the partial contributions $I_{l,m}$ to the absorption cross section due to final states with orbital angular momentum l,m,

$$I_\perp(\omega)=I_{2,2}(\omega)+\tfrac{1}{6}I_{2,0}(\omega)+\tfrac{1}{2}I_{2,1}(\omega) .$$

The unpolarized spectrum is given by

$$I(\omega)=\tfrac{2}{3}I_\perp(\omega)+\tfrac{1}{3}I_\|(\omega)$$
$$=\tfrac{1}{3}[2I_{2,2}(\omega)+I_{2,0}(\omega)+2I_{2,1}(\omega)] .$$

In Fig. 5 the polarized $2p\rightarrow3d$ spectra are reported. Only transitions above the Fermi level at 11.6 eV indicated by the dashed line are allowed. The white line is clearly due mainly to the $\mathbf{E}\perp c$ polarization, but beyond 12.5 eV, i.e., at about 1 eV above the Fermi level, the unoccu-

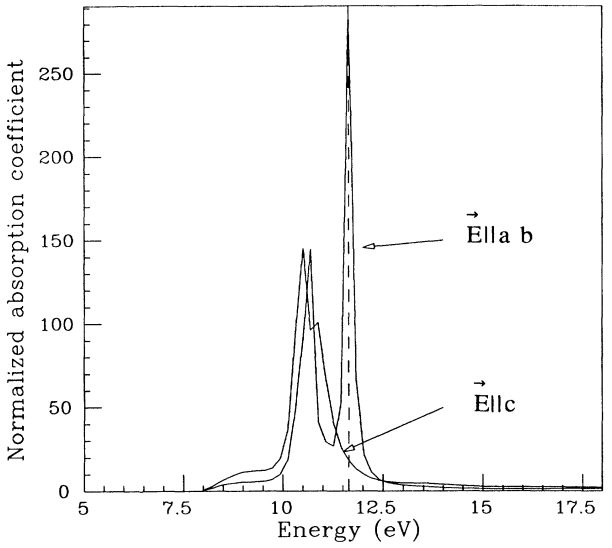

FIG. 5. Calculated polarized $\mathbf{E}\|c$ and $E\|ab$ ($\mathbf{E}\perp c$) Cu L_3-edge XANES spectra of $Bi_2Sr_2CaCu_2O_{8+\delta}$ for a cluster of five shells as shown in Fig. 2. The transitions to occupied and unoccupied Cu $3d$ valence states are calculated. The Fermi level is close to the maximum of the highest-energy peak (dashed line).

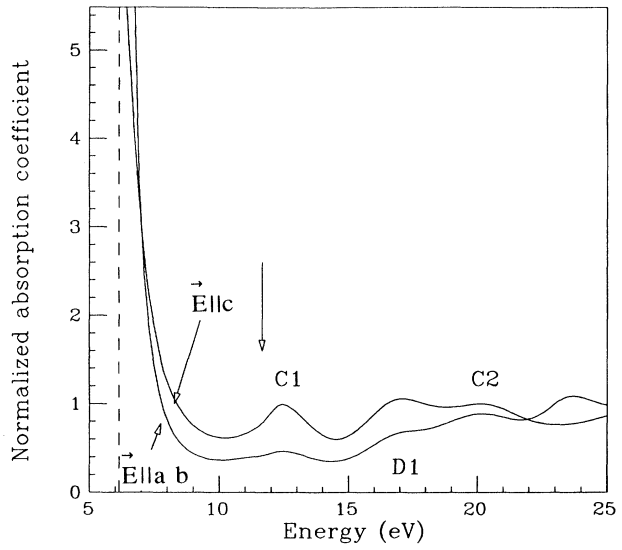

FIG. 7. Calculated absorption coefficient, using the $Z+1$ approximation for the fully relaxed potential, for the polarized $\mathbf{E}\|ab$ ($\mathbf{E}\perp c$) and $\mathbf{E}\|c$ Cu L_3-edge XANES spectra of $Bi_2Sr_2CaCu_2O_{8+\delta}$ for the $2p\rightarrow\varepsilon d$ transitions to final states in the continuum (ε) above the Fermi level.

pied states in the continuum are predicted to have mainly $m_l=0$ character. In Fig. 6 we plot the calculated polarized $\mathbf{E}\|c$ and $\mathbf{E}\perp c$ XANES spectra for transitions in the continuum above the Fermi level. The polarized spectra for the fully relaxed potential, using the $Z+1$ approximation is shown in Fig. 7.

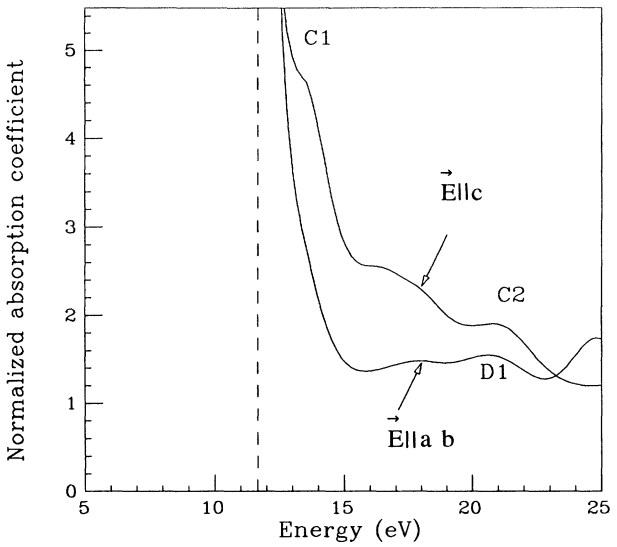

FIG. 6. Calculated polarized $\mathbf{E}\|c$ and $E\|ab$ ($\mathbf{E}\perp c$) Cu L_3-edge XANES spectra of $Bi_2Sr_2CaCu_2O_{8+\delta}$ for the $2p\rightarrow\varepsilon d$ transitions to final states in the continuum (ε) above the Fermi level. The absorption coefficient has been normalized to the value of the atomic absorption coefficient for the central Cu ion at high energy $\alpha_{0\infty}$.

E. Comparison between the calculated and experimental spectra

In order to compare the calculated spectrum with the experimental data we have to introduce in the calculation the broadening due to the experimental resolution the core-hole life time and finally the energy-dependent photoelectron lifetime due to the inelastic scattering with valence electrons. The inelastic scattering due to valence electron-hole excitations and plasmons reduce the amplitude of the elastic channel contributing to the XANES spectrum.

In Fig. 8 the different contributions to the total

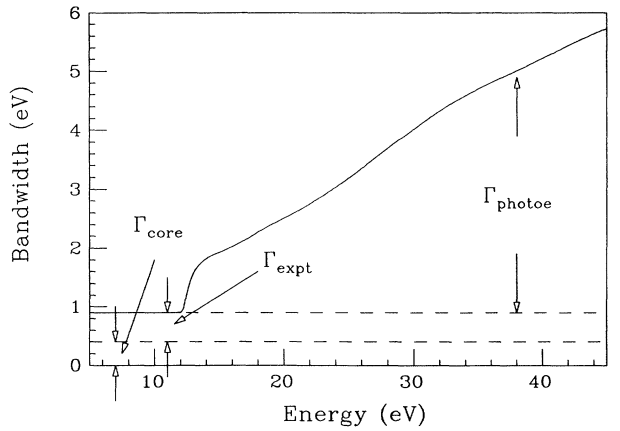

FIG. 8. Energy bandwidth of final states in the Cu L_3-edge XANES due to the core-hole lifetime, experimental resolution, and photoelectron lifetime due to the inelastic scattering of the excited photoelectron.

broadening term are shown. The energy-dependent bandwidth function (due to the photoelectron lifetime) should be zero for bound states below the Fermi level, and jumps are expected at the energy of plasmon excitations.[55] In the present case it has been found by fixing the zero at the Fermi level, and it has been extracted from the integral of the electron energy loss function in the range from 0 to 40 eV.[56] This procedure gives a qualitative estimate of the energy-dependent bandwidth function, but its actual values are adjusted by looking for the agreement with the experimental data.

The calculated polarized Cu L_3-XANES spectra are shown in Figs. 9 and 10 for the fully relaxed potential. The transition to the unoccupied Cu $3d$ valence states gives the white line at 6.1 eV above the intersphere energy, which is a bound state at 5.5 below the continuum threshold E_0. The $\mathbf{E}\|c$ calculated spectrum shows a component of the white line, which is about 10% of the total oscillator strength of the Cu $2p \rightarrow 3d$ transitions. The energy position of the white line in the two polarizations is predicted to be the same. The component of the white line in the $\mathbf{E}\|c$ spectrum is expected because of the pseudo-Jahn-Teller distortion of the Cu square pyramid coordination, which mixes the $m_l=2$ with the $m_l=0$ states in agreement with early x-ray-absorption calculations for a small Cu cluster.[57]

The comparison between the experimental spectra and the theoretical spectra (see Table III and Fig. 10) show first that the best agreement is found with the calculation in the fully relaxed potential, obtained by using the $Z+1$ approximation. The most direct experimental evidence is that given by the energy separation between the peak $C1$ and the white line that in the experimental spectra is at 5.2 eV, while in the calculated spectra it is 6.3 eV and 2.1 eV in the fully relaxed or in the unrelaxed potential, respectively.

The validity of the fully relaxed potential for the prediction of the XANES spectra[1] is well established for electronic transitions to nearly empty bands, and it is known as the final-state rule.[58] The final-state rule has been questioned for the case of transitions in the nearly filled band limit, which is the case for the $2p \rightarrow 3d$ transitions in Cu, where the final state gives a completely filled shell $2p^5 3d^{10}$ in the insulating system or a nearly filled shell in the metallic phase $2p^5 3d^{10} \underline{L}(k)$.[59,60] Therefore, while the $Z+1$ approximation was expected to be valid for the transitions to the unoccupied state in the continuum, it was expected to break down for the white line prediction. On the contrary, the present work shows that the $2p \rightarrow 3d$ transitions in this Cu compound are also well predicted by the final-state $Z+1$ approximation.

Moreover the agreement between the calculated and the experimental energy separation between the white line and the peak $C1$ shows that the calculated Coulomb interaction 5.5 eV between the Cu $2p$ core hole and the Cu $3d$ electron is correct within 1 eV.

The feature in the continuum $C1$ at 936.5 eV is well predicted by the calculation; a second peak at 939.5 eV is not predicted by the present calculation; the third feature, $C2$, which appears as a broad band extending from 943 to 946 eV is predicted by the calculation but at lower energy. The peak $D1$ of the in-plane polarized spectrum is weak, but we have found it in all samples that we have measured, and in some spectra it was better resolved. It is well predicted by the calculated $\mathbf{E}\|ab$ spectrum as well as the minimum at 939 eV.

The main disagreement between the calculation and the experiment concerns the peak at 939.5 eV measured for the out-of-plane polarization. This peak was also ob-

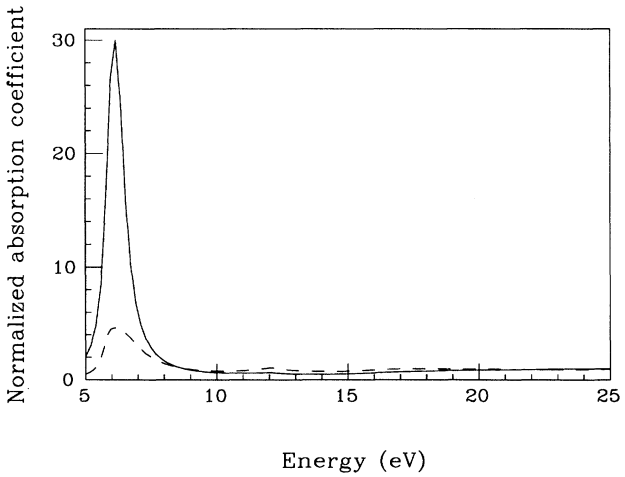

FIG. 9. Calculated polarized $\mathbf{E}\|ab$ ($\mathbf{E}\perp c$) (solid line) and $\mathbf{E}\|c$ (dashed line) Cu L_3-edge XANES of $Bi_2Sr_2CaCu_2O_{8+\delta}$ including the energy-dependent broadening (shown in Fig. 8) in the fully relaxed potential (shown in Fig. 7). This calculated spectrum has to be compared with the experimental spectrum in Fig. 1.

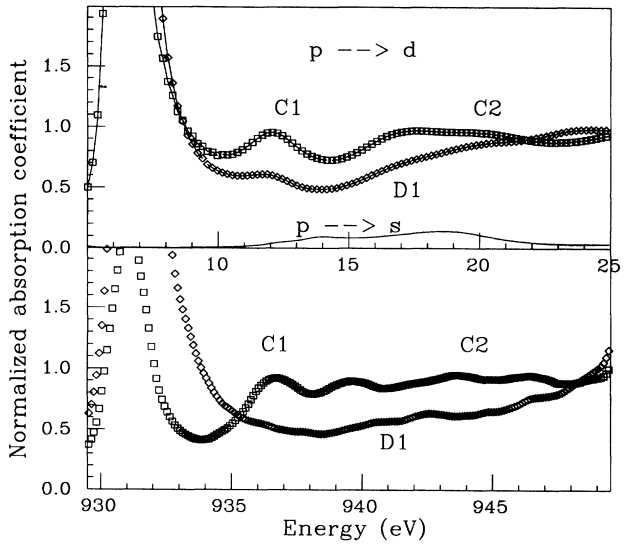

FIG. 10. Calculated cross section for the $1p \rightarrow s$ channel contributing to the Cu L_3-edge XANES spectrum of $Bi_2Sr_2CaCu_2O_{8+\delta}$ and a blowup of the polarized spectra for transitions to the continuum states, including the energy-dependent broadening in the fully relaxed potential. In the lower panel the blowup of the experimental polarized XANES spectra is shown for comparison.

served recently by Abbate *et al.*[61] and by Pompa *et al.* in the bulk XANES measurement of an oriented film by the fluorescence mode.[62] This peak is at the energy of the expected Cu $2p^5 3d^9$ final state due to some probability for the Cu $3d^8$ configuration in the ground state. Further work comparing the insulating with metallic phase is in process to establish if this peak is growing with doping or it is due to a multielectron final-state feature.[13–15,55]

The comparison of the experimental XANES spectrum in the continuum and the calculated spectrum shown in Fig. 10 is satisfactory, taking into account that the coordinates of the atoms of the cluster taken from Bordet *et al.* are only averaged values over the five different Cu sites present in the real structure of $Bi_2Sr_2CaCu_2O_{8+\delta}$, which exhibits a 5×1 superstructure.[31] In fact a disagreement between experiment and calculation is found in the range between 938–941 eV. However, the calculation predicts the correct experimental dichroism of the XANES spectra and the main features $C1$, $C2$, and $D1$. By comparing the calculated and the experimental curves in Fig. 10, the continuum threshold E_0 is identified at about 936.5±1 eV in the Cu L_3-edge XANES.

Several authors have assigned the weak-absorption peaks in the continuum to the $2p\rightarrow s$ channel allowed by the dipole selection rules $\Delta l=-1$. We have found that this assignment is not correct by calculating the contribution of the $2p\rightarrow s$ channel. The results of the present calculations for the $p\rightarrow s$ absorption cross section are reported in Fig. 10. The results show that this contribution is really negligible; in fact, the oscillator strength for this channel is close to zero in the white line energy range, and it is about one order of magnitude smaller than the $2p\rightarrow\varepsilon d$ channel in the continuum XANES range, showing that the strength of the $2p\rightarrow s$ channel is at its maximum at two orders of magnitude smaller than the oscillator strength for the $2p\rightarrow 3d$ transitions.

Finally we would like to discuss the comparison between the experimental and the calculated white line. The extended investigation of several cleaved Bi-Ca-Sr-Cu-O single crystals, oriented pellets, and films that show the characteristic 2:2:1:2 crystallographic single-phase and a single resistive jump at the critical temperature show that the energy position of the $\mathbf{E}\|ab$ white line is doping dependent, and it appears in the range from the energy position of the white line of CuO (931.2 eV) up to ~200 meV above it. Also the energy position of the $\mathbf{E}\|c$ white line moves from ~931.1 eV, in the insulating systems obtained by Y to Ca substitution, toward higher energy. Therefore the energy splitting Δz between the in-plane and out-of-plane polarization can range from ~400±100 meV to ~100±100 meV. The polarized white line spectrum reported in Fig. 1 shows a typical spectrum of the 2:2:1:2 sample, where the $\mathbf{E}\|c$ white line is at 100 meV below the CuO white line and the $\mathbf{E}\|ab$ white line is at about 100 meV above it. Considering the 900 meV of the white line width, the energy splitting of 100 meV is close to zero. Therefore because the energy splitting is doping dependent, the results of our investigation are not in contradiction with either the data of Nüker *et al.*[63] measured by electron energy loss, who have reported no energy splitting, or with the data by Abbate *et al.*,[61] who reported for a Pb-doped sample a 500-meV energy splitting. In fact, these values are the limits between which we have found that the energy splitting changes with different dopants, and by taking into account the broadening of the white line and an error of 100 meV in the energy splitting measurement. The present results are also in agreement with our early report of Δz as 400–300 meV (Ref. 23) or with the recent soft x-ray-absorption measurement probing the bulk by using the soft x-ray fluorescence yield by Pompa *et al.*,[62] giving an energy splitting of 150 meV.

In order to show the experimental situation we have compared the polarized white lines detected in different samples by different techniques in Fig. 11. The reason for the differences shown in Fig. 11 are not due to the detection techniques but to intrinsic differences of the samples; similar differences can be observed by studying different samples by using the total electron yield. In fact, we have found that polarized white lines change their intensity and energy position not with doping but with the type of dopants. Also the 2:2:1:2 samples can be quite different, with the c axis ranging from 30.6 to 30.95 Å, with 25% Y substituting for Ca, with Pb doping (as it was in the case of the sample studied by Abbate *et al.*), with different heat treatments changing oxygen concentration, with a different Ca/Sr ratio, and so on. In fact, the local site structure of the five different Cu sites, giving the nearly 5×1 superstructure with largely different distortions can be dependent on the dopants.

The energy shift of the $\mathbf{E}\|c$ white line is here assigned to the impurity states formed in the correlation gap by the dopants, and therefore it is sensitive to the doping level and on the actual dopants inducing different distortions of the Cu sites. Further systematic work on well-

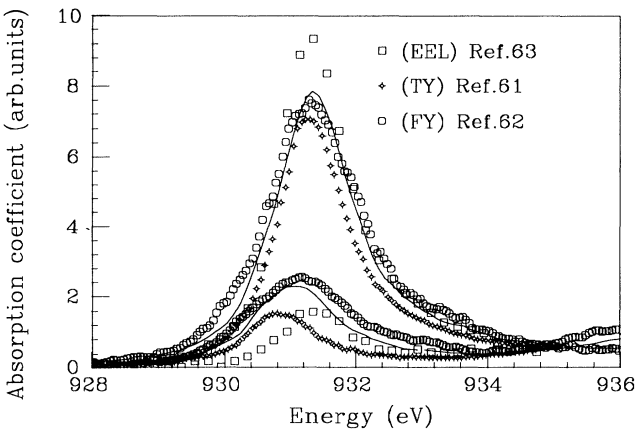

FIG. 11. Polarized Cu L_3-edge white lines of Bi-Sr-Ca-CuO samples with 2:2:1:2 crystallographic phase reported in the present work (solid line), compared with the spectra measured in fluorescence yield (FY) mode by Pompa *et al.* (Ref. 62) (empty circles), by total electron yield (TY) by Abbate *et al.* (Ref. 61) (stars), and by electron-energy loss (EEL) by Nüker *et al.* (Ref. 63) (squares). The peaks of the $\mathbf{E}\|ab$ white lines are in the range 7–10 in arbitrary units in the figure and the peaks of the $\mathbf{E}\|c$ white lines are in the range 1.5–2.5.

characterized samples is necessary to fully understand how these states are correlated with doping.

The $\mathbf{E}\|ab$ white line of all metallic 2:2:1:2 phase crystals shows the characteristic asymmetric white line. The agreement between several authors on the line shape is good, as shown in Fig. 11. Because of the different calibration of the energy scale of different authors, we have aligned the energy position of the $\mathbf{E}\|ab$ white lines of different authors in Fig. 11 at the same energy for comparison. We have found that the energy position of the white line shows a blue shift with increasing doping, and also this effect contributes to the different values of the energy shift Δz reported by different authors and found in different samples.

Finally the relative number of the Cu $3d_{z^2}$ holes n_z on the total number of the Cu $3d$ holes has been extracted from the Cu L_3 absorption spectra. It is given by the integral of the absorption spectrum over the energy range of the bound states below the continuum threshold:

$$n_z = \int I_{2,0}(\omega)d\omega \Big/ \int [2I_{2,2}(\omega)+I_{2,0}(\omega)+2I_{2,1}(\omega)]d\omega$$
$$= \tfrac{1}{2}\left[\int I_{\|}(\omega)d\omega \Big/ \int I(\omega)d\omega\right],$$

i.e., one half of the ratio between the integral of the $\mathbf{E}\|c$ polarized spectrum and the integral of the unpolarized spectrum, assuming a negligible contribution of the unoccupied $m_l=1$ states to the $\mathbf{E}\|c$ polarized spectrum. The integrals are calculated in the range of the bound states below the continuum threshold, where all unoccupied Cu $3d$ states are pulled down by the core-hole final-state effect. We have calculated the integrals over the energy range of 928–935.5 eV by fixing the higher-energy limit to the isosbestic point. We have found a value of n_z ranging from 15±2 % to 20±2 % in different samples, and it is in qualitative agreement with Nüker *et al.*[63] and Abbate *et al.*[6] Taking into account that in the insulating crystals obtained by Y to Ca substitution a value of $n_z=8\%$ was found[23–25] and that the absolute number of n_z can be affected by systematic errors due to incomplete polarization of the x-ray beam, we estimate that about 7–12% of the weight of the Cu $m_l=0$ holes is associated with the itinerant ligand holes.

The calculated $\mathbf{E}\|c$ white line in Fig. 9 is at the same energy position as the $\mathbf{E}\|ab$ white line, and it can be considered as the prediction of the probability of $m_l=0$ components in the mainly $m_l=2$ band crossing the Fermi level due to Cu site distortion.

The $\mathbf{E}\|c$ white line at lower energy than the CuO white line can be partially associated to impurity states $3d^9_{3z^2-r}\underline{L}(a_1)$ in the correlation gap formed by the dopants that are present also in the insulating phase at low doping level that are not included in our calculation. By increasing the doping at the insulating-to-metal transitions additional itinerant $3d^9_{3z^2-r^2}\underline{L}(k)$ states are formed at the same time as the singlet states $3d^9_{x^2-y^2}\underline{L}(k)$ states giving the high-energy tail of the $\mathbf{E}\|ab$ white line. The interplay between the band formed by the impurity band and the Zhang-Rice singlet states formed by doping is probably the reason for the modulation of the energy splitting between the out-of-plane and in-plane polarized white line. An extended investigation of many crystals with different doping and the effect of the transition from the insulating-to-metallic phase on the polarized white lines is in process to clarify this key aspect of the electronic structure of high-T_c superconductors.

IV. CONCLUSIONS

In conclusion, we have interpreted the experimental features of the Cu L_3-edge polarized XANES spectrum of $Bi_2Sr_2CaCu_2O_{8+\delta}$. We have identified the physical origin of the peaks C_1 and C_2 in the continuum. The interpretation of the XANES of $Bi_2Sr_2CaCu_2O_{8+\delta}$ in terms of a one-electron approximation shows that the high-energy bands beyond the Cu $3d_{x^2-y^2}$ band does not evidence electron correlation effects. The oscillator strength for the $2p\rightarrow s$ channel is shown to be negligible. The $Z+1$ approximation describing the fully relaxed final-state potential is shown to be valid also for the $2p\rightarrow 3d$ transitions in the nearly filled band limit. The electron-hole Coulomb interaction in the final states splits off the Cu $3d$ unoccupied states from the continuum states εd of the high-energy conduction bands. The integral of the polarized spectra is shown to give a measure of the relative weight of the Cu $3d_{z^2}$ unoccupied states.

ACKNOWLEDGMENTS

The present research was supported by the Consorzio Interuniversitario Nazionale per la Fisica della Materia (INFM) and Consiglio Nazionale delle Richerche, in the framework of the *progetto finalizzato per le tecnologie superconduttive.* We thank Dr. P. Castrucci, and Dr. A. Fabrizi for help in the experiment and in the data analysis. We are grateful to Dr. H. Katayama-Yoshida for the $Bi_2Sr_2CaCu_2O_{8+\delta}$ single crystal. We acknowledge useful discussions with Dr. C. R. Natoli. We thank the director and the staff of the synchrotron radiation facility LURE for the beam time and support in the framework of the CEE program for the large European facilities. One of us (D. U.) acknowledges financial support by a CEE grant within the CODEST program. One of us (C.L.) would like to thank the INFM for support during his visit in Italy.

*Mailing address: Research Unit of INFM, Department of Physics, University of Rome "La Sapienza," I-00485 Rome, Italy.

†Permanent address: Institute of Physics, Academia Sinica, Beijing, China.

[1] A. Bianconi, in *X-ray Absorption: Principles, Applications, Techniques of EXAFS, SEXAFS, and XANES,* edited by D. C. Koningsberger and R. Prinz (Wiley, New York, 1988), p. 573.

[2] A. Bianconi, J. Garcia, and M. Benfatto, in *Synchrotron Radiation in Chemistry and Biology I,* Topics in Current Chemistry,

Vol. 145, edited by E. Mandelkow (Springer-Verlag, Berlin, 1988), p. 29.
[3]P. J. Durham, in *X-ray Absorption: Principles, Applications, Techniques of EXAFS, SEXAFS, and XANES* (Ref. 1), p. 53.
[4]P. J. Durham, J. B. Pendry, and C. H. Hodges, Comput. Phys. Commun. **25**, 193 (1982).
[5]J. G. Bednorz and K. A. Müller, Z. Phys. B **64**, 189 (1986).
[6]J. G. Bednorz and K. A. Müller, Rev. Mod. Phys. **60**, 565 (1988).
[7]W. E. Pickett, Rev. Mod. Phys. **61**, 433 (1989).
[8]*High T_c Superconductors: Electronic Structure,* edited by A. Bianconi and A. Marcelli (Pergamon, Oxford, 1989).
[9]*Earlier and Recent Aspects of Superconductivity,* Springer Series in Solid State Sciences, edited by K. A. Müller and J. G. Bednorz (Springer-Verlag, Berlin, 1990).
[10]K. Yvon and M. Francois, Z. Phys. **76**, 413 (1989).
[11]K. Garg, A. Bianconi, S. Della Longa, A. Clozza, M. De Santis, and A. Marcelli, Phys. Rev. B **38**, 244 (1988).
[12]S. Della Longa, M. De Simone, C. Li, M. Pompa, and A. Bianconi, in *High T_c Superconductors: Electronic Structure,* (Ref. 8), p. 259.
[13]J. Guo, D. E. Ellis, G. L. Goodman, E. E. Alp, L. Soderholm, and G. K. Shenoy, Phys. Rev. B **41**, 82 (1990).
[14]A. Bianconi, C. Li, F. Campanella, S. Della Longa, I. Pettiti, M. Pompa, S. Turtú, and D. Udron, Phys. Rev. B **44**, 4560 (1991).
[15]C. Li, M. Pompa, A. Congiu Castellano, S. Della Longa, A. Bianconi, Physica C **175**, 379 (1991).
[16]T. A. Tyson, D. A. Case, B. Hedman, and K. O. Hodgson (unpublished).
[17]A. Bianconi, A. Congiu-Castellano, M. De Santis, P. Rudolf, A. M. Flank, P. Lagarde, and A. Marcelli, Solid State Commun. **63**, 1009 (1987).
[18]A. Bianconi, J. Budnick, A. M. Flnak, A. Fontaine, P. Lagarde, A. Marcelli, H. Tolentino, B. Chamberland, C. Michel, B. Raveau, and G. Demazeau, Phys. Lett. **127**, 285 (1988).
[19]D. D. Sarma, O. Strebel, C. T. Simmons, U. Neukirch, G. Kaindl, R. Hoppe, and H. P. Müller, Phys. Rev. B **37**, 9784 (1988).
[20]M. Ronay, A. Santoni, A. G. Schrott, L. J. Terminello, S. P. Kowalczyk, and F. J. Himpsel, Solid State Commun. **77**, 699 (1991).
[21]A. Bianconi, M. De Santis, A. M. Flank, A. Fontaine, P. Lagarde, A. Marcelli, H. Katayama-Yoshida, and A. Kotani, Physica C **153-155**, 1760 (1988). A. Bianconi, M. De Santis, A. Di Cicco, A. M. Flank, A. Fontaine, P. Lagarde, H. Katayama-Yoshida, A. Kotani, and A. Marcelli, Phys. Rev. B **38**, 7196 (1988).
[22]A. Bianconi, P. Castrucci, M. De Santis, A. Di Cicco, A. Fabrizi, A. M. Flank, P. Lagarde, H. Katayama Yoshida, A. Kotani, A. Marcelli, Z. Zhao, and C. Politis, Mod. Phys. Lett. **2**, 1313 (1988); A. Bianconi, P. Castrucci, M. De Santis, A. Di Cicco, A. M. Flank, P. Lagarde, S. Della Longa, A. Marcelli, Y. Endoh, H. Katayama Yoshida, and Z. X. Zhao, in *High T_c Superconductors: Electronic Structure* (Ref. 8), p. 281.
[23]A. Biaconi, P. Castrucci, A. Fabrizi, M. Pompa, A. M. Flank, P. Lagarde, H. Katayama-Yoshida, and G. Calestani, in *Earlier and Recent Aspects of Superconductivity,* Springer Series in Solid State Sciences, edited by K. A. Müller and J. G. Bednorz, (Springer-Verlag, Berlin, 1990), p. 407.
[24]A. Bianconi, P. Castrucci, A. Fabrizi, M. Pompa, A. M. Flank, P. Lagarde, H. Katayama-Yoshida, G. Calestani, Physica C **162-164**, 209 (1990).
[25]A. Bianconi, in *International Conference on Superconductivity-ICSC, Proceedings of the International Conference on Superconductivity, Bangalore, 1990,* edited by S. K. Joshi, C. N. R. Rao, and S. V. Subranyam (World Scientific, Singapore (1990), p. 448.
[26]F. C. Zhang and T. M. Rice, Phys. Rev. B **37**, 3759 (1988).
[27]H. Maeda, Y. Tanaka, M. Fukutomi, and T. Asano Jpn. J. Appl. Phys. **27**, L209 (1988).
[28]A. W. Sleight, Science **242**, 1519 (1988).
[29]P. Bordet, J. J. Capponi, C. Chaillout, A. W. Hewat, E. A. Hewat, J. L. Houdeau, M. Marezio, J. L. Tholence, and D. Tranqui, Physica C **156**, 189 (1988).
[30]M. A. Subramanian, C. C. Torardi, J. C. Calabrese, J. Gopalakrishan, K. J. Morrisey, T. R. Askew, R. B. Flippen, U. Chowdhry, and A. W. Sleight, Science **239**, 1015 (1988).
[31]G. Calestani, C. Rizzoli, M. G. Francesconi, and G. D. Andreetti, Physica C **161**, 598 (1989); M. Onoda, and M. Sato, Solid State Commun. **67**, 799 (1988).
[32]K. Yvon and M. Francois, Z. Phys. **76**, 413 (1989).
[33]P. P. Lottici, G. Antonioli, and F. Licci, Physica C **152**, 468 (1988).
[34]A. Bianconi, P. Castrucci, M. De Simone, A. Di Cicco, A. Fabrizi, C. Li, M. Pompa, D. Udron, A. M. Flank, P. Lagarde, and G. Calestani, in *High T_c Superconductivity, SATT 3,* edited by C. Ferdeghini and A. S. Siri (World Scientific, Singapore, 1990), p. 144.
[35]J. Röhler and A. Larish, in *Electronic Properties of High-T_c Superconductors and Related Compounds,* Springer Series in Solid State Sciences,Vol. 99, edited by H. Kuzmany and M. Mehring (Springer-Verlag, Berlin, 1990), p. 152.
[36]T. Takahashi, H. Matsuyama, H. Katayama-Yoshida, Y. Okabe, S. Hosoya, K. Seki, H. Fujimoto, M. Sato, and H. Inokuchi, Nature (London) **334**, 691 (1988); Phys. Rev. B **39**, 6636 (1989).
[37]C. G. Olson, R. Liu, A.-B. Yang, D. W. Lynch A. J. Arko, R. S. List, B. W. Veal, Y. C. Chang, P. Z. Jiang, and A. P. Pauliskas, Science **245**, 731 (1989).
[38]P. Calvani, M. Capizzi, S. Lupi, P. Maselli, D. Peschiaroli, and H. Katayama-Yoshida Solid State Commun. **74**, 1333 (1990).
[39]M. S. Hybertsen and L. F. Mattheis, Phys. Rev. Lett. **60**, 1661 (1988).
[40]H. Krakauer and W. E. Pickett, Phys. Rev. Lett. **60**, 1665 (1988).
[41]S. Masidda, J. Yu, and A. J. Freeman, Physica C **152**, 251 (1988).
[42]P. Marksteiner, S. Massida, J. Yu, A. J. Freeman, and J. Redinger, Phys. Rev. B **38**, 5098 (1988).
[43]F. Herman, R. V. Kasowski, and W. Y. Hsu, Phys. Rev. B **38**, 204 (1988).
[44]A. Bianconi, A. Congiu Castellano, M. De Santis, P. Delogu, A. Gargano, and R. Giorgi, Solid State Commun. **63**, 1135 (1987).
[45]A. Bianconi, A. Clozza, A. Congiu Castellano, S. Della Longa, M. De Santis, A. Di Cicco, K. Garg, P. Delogu, A. Gargano, R. Giorgi, P. Lagarde, A. M. Flank, and A. Marcelli, in *Progress in High Temperature Superconductivity,* edited by S. Lundquist, E. Tosatti, M. Tosi, and Y. Lu (World Scientific, Singapore, 1987); Int. J. Mod. Phys. **1**, 205 (1987).
[46]M. De Santis, A. Bianconi, A. Clozza, P. Castrucci, A. Di Cicco, M. De Simone, A. M. Flank, P. Lagarde, J. Budnick, P. Delogu, A. Gargano, R. Giorgi, and T. D. Makris, in *High T_c Superconductors: Electronic Structure* (Ref. 8), p. 313.

[47]Z.-X. Shen, J. W. Allen, J.-J. Yeh, J.-S. Kang, W. Ellis, W. E. Spicer, I. Lindau, M. B. Maple, Y. D. Dalichaouch, M. S. Torikachvili, J. Z. Sun, and T. H. Geballe, Phys. Rev. B **36**, 8414 (1987).

[48]G. Van der Laan and B. T. Thole, J. Electron. Spectrosc. Relat. Phenom. **46**, 123 (1988).

[49]P. G. Burke, N. Chandra, and F. A. Gianturco, J. Phys. B **5**, 2212 (1972).

[50]N. Chandra, J. Phys. B **20**, 3405 (1987).

[51]K. H. Johnson, Adv. Quantum. Chem. **7**, 143 (1973).

[52]J. B. Diamond, Chem. Phys. Lett. **20**, 63 (1973).

[53]F. W. Kutzler, C. R. Natoli, D. K. Misemer, S. Doniach, and K. O. Hodgson, J. Chem. Phys. **73**, 3274 (1980).

[54]I. Landau and E. Lifchitz, *Mecanique Quantique Theorie Non Relativiste* (Mir, Moscow, 1966), p. 470.

[55]A. Bianconi, J. Garcia, M. Benfatto, A. Marcelli, C. R. Natoli, and M. F. Ruiz-Lopez, Phys. Rev. B **43**, 6885 (1991).

[56]J. Fink, N. Nucker, H. Romberg, and S. Nakai, in *High T_c Superconductors: Electronic Structure* (Ref. 8), p. 293.

[57]Y. Seino, A. Kotani, and A. Bianconi, J. Phys. Soc. Jpn. **59**, 815 (1990).

[58]U. von Barth and G. Grossman Phys. Scr. **21**, 580 (1980); **28**, 107 (1983); Solid State Commun. **32**, 645, (1979); Phys. Rev. B **25**, 5150 (1982).

[59]E. A. Stern and J. J. Rehr, Phys. Rev. B **27**, 3351 (1983).

[60]J. Zanen, M. Alouani, and O. Jepsen, Phys. Rev. B **40**, 837 (1989).

[61]M. Abbate, M. Sacchi, J. J. Wnuk, L. W. M. Schreurs, Y. S. Wang, R. Lof, and J. C. Fuggle, Phys. Rev. **42**, 7914 (1990).

[62]M. Pompa, A. Fabrizi, H. Katayama-Yoshida, and A. Bianconi (unpublished).

[63]N. Nüker, H. Romberg, X. X. Xi, J. Fink, B. Gegenheimer, and Z. X. Zhao, Phys. Rev. B **39**, 6619 (1989).